Stability analysis of a diode-pumped, thermal birefringence-compensated two-rod Nd:YAG laser with 770-W output power

Sungman Lee, Mijeong Yun, Byung Heon Cha, Cheol Joong Kim, Sungsoo Suk, and Hyun Su Kim

Using a ray matrix method, we analyze theoretically how the r and θ polarizations affect the resonator stability condition of two laser heads with or without thermal birefringence compensation. The resonator stability condition is analyzed graphically for a plane–parallel and a concave–concave resonator. The maximum range of stable region is found for both the short and the long cavity. The characteristics of the laser output power are confirmed experimentally in association with the resonator stability condition. The laser output power of 776 W is obtained with the optical-to-optical efficiency of 45% for a plane–parallel resonator with a short crystal separation.

OCIS codes: 140.3410, 140.3480, 140.3530.

1. Introduction

For the development of a diode-pumped high-power solid-state laser, a series of laser heads have been used in general with and without thermal birefringence compensation. For example, Akiyama *et al.*[1] used three laser heads to obtain a output power of 5.4 kW cw without the birefringence compensation. A resonator with two laser heads and a 90° quartz rotator in between was used for the thermal birefringence compensation of the crystal rod.[2] In the side-pumped Nd:YAG laser, at the high-input pump power, the crystal rod has a short thermal focal length for the crystal rod with a small diameter. Therefore the detailed analysis of the resonator stability condition depending on both mirror distances and a crystal separation is essential for the achievement of a high-output power with good stability, isotropic beam profile, and high optical efficiency.

For the resonator with two laser heads, a general relation between the radius of the fundamental mode and the stability of the resonator was reported previously.[3] In addition, in the same article, the stable range of the stability condition was calculated theoretically in the various distances of resonator mirrors and crystal separation. However, thermal birefringence compensation for the r and θ polarizations was not considered in the analysis of the stability condition. In the design of a resonator with two laser heads, the thermal birefringence compensation with a 90° quartz rotator was reported experimentally to provide higher output power with better output power stability, compared with that the case of no thermal birefringence compensation.[2] Recently, for a single laser head, the stability condition including the r and θ polarizations was calculated theoretically with a ray-matrix method and analyzed experimentally in terms of the laser pump power and the distance of the resonator mirrors.[4] However, the stability condition for two pump heads must be analyzed to scale up a laser output power with several laser heads with or without thermal birefringence compensation.

In this article, for two laser heads, we analyze theoretically with a ray-matrix method the effects of the r and θ polarizations on the resonator stability condition with or without thermal birefringence compensation. The resonator stability conditions of a plane–parallel and a concave–concave resonator are analyzed graphically in detail in terms of the total pump power of two laser heads and the distance of an output coupler. We show how the stable resonator

S. Lee (smlee3@kaeri.re.kr), M. Yun, B.-H. Cha, and C.-J. Kim are with the Korea Atomic Energy Research Institute, Taejon 305-600, Korea. S. Suk is with the Department of Physics, Kyungpook National University, Taegu 702-701, Korea. H.-S. Kim is with the Department of Photonics Engineering, Chosun University, Gwangju 501-759, Korea.

Received 2 January 2002; revised manuscript received 2 July 2002.

0003-6935/02/275625-07$15.00/0

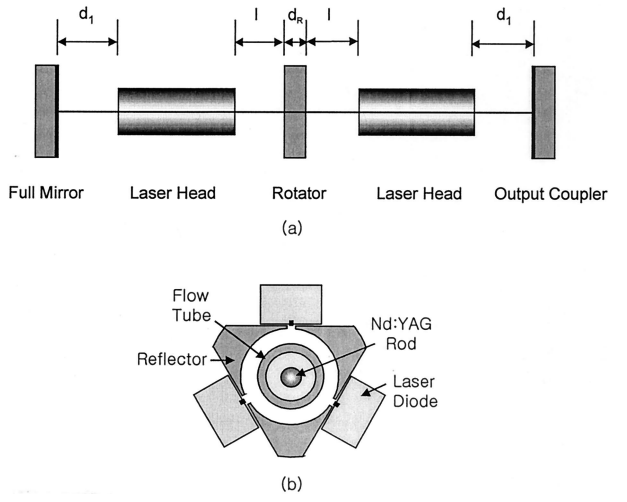

Fig. 1. (a) Thermal birefringence compensated resonator scheme of a plane-parallel resonator, including two crystal rods and a 90° rotator in between; (b) schematic diagram of the laser pump head.

condition and the maximum range of stable region are modified for both the short and the long cavity of a plane–parallel resonator and for a concave–concave resonator. In addition, the characteristics of the laser output power are confirmed experimentally in association with the calculated resonator stability condition. In particular, the maximum laser output power of 776 W, which corresponds to the optical-to-optical efficiency of 45% and the optical slope efficiency of 69%, is obtained for the symmetric plane–parallel resonator with the shortest crystal gap distance.

2. Analysis of Stability Condition

The resonator scheme used for the stability analysis is shown in Fig. 1(a) and consists of two crystal rods and a 90° quartz rotator in between for thermal birefringence compensation. Two diode-pumped Nd:YAG laser heads have the schematic geometry shown in Fig. 1(b), and each head is constructed with a Nd:YAG rod having a diameter of 5 mm and doping concentration of 0.6 at. %, a cooling sleeve, a diffusive optical cavity, and three diode arrays having a summed pump power of 1080 W. The length of the laser active medium is 9.6 cm. The detailed geometry of the laser head is described in a report by Lee *et al.*[5]

For the analysis of the resonator stability condition, we need to determine the thermal focal length of single laser head for r and θ polarizations. For such purpose, the average thermal focal length (f) of a single laser head is measured for the varied input pump power (P_{in}) by use of a He–Ne laser at lasing condition. For the measurement, an output coupler has a reflectance of 65%. From the plot between $1/f$ and P_{in}, we find the relation $1/f \approx 8.73P_{\text{in}} - 1$, and determine the slope of reciprocal thermal focal length as $8.73D/\text{kW}$.[4] Here, D is a diopter and has a unit of m^{-1}. To calculate f_r and f_θ, we used the ratio of theoretical thermal focal length $f_\theta/f_r \approx 1.2$ (Ref. 6) and the definition of average thermal focal length $f = (f_r + f_\theta)/2$. Then, by the above relation $1/f \approx 8.73P_{\text{in}} - 1$, we can determine f_r and f_θ.

The stability conditions as parameters of the total pump power of two laser heads, the distance between two crystal rods, and the distances between the crystal rod and the laser mirror are calculated theoretically. A uniformly heated laser active element has parabolic temperature distribution, and the ray matrix $\mathbf{M}_{r,\theta}$ for the medium is described as follows:[7]

$$\mathbf{M}_{r,\theta} = \begin{bmatrix} \cos \Gamma_{r,\theta} L & (n_0 \Gamma_{r,\theta})^{-1} \sin \Gamma_{r,\theta} L \\ -n_0 \Gamma_{r,\theta} \sin \Gamma_{r,\theta} L & \cos \Gamma_{r,\theta} L \end{bmatrix}, \quad (1)$$

where $\Gamma_{r,\theta} = (n_{2r,2\theta}/n_0)^{1/2}$, L is the length of the laser active medium, and n_0 is the refractive index at the center of the rod. The $n_{2r,2\theta}$ is given by the relation

$$n_{2r,2\theta} = n_0 \frac{4\Delta T}{R^2} \left(\frac{1}{2n_0} \frac{dn}{dT} + n_0{}^2 \alpha C_{r,\theta} \right), \quad (2)$$

where R is the radius of the crystal rod, dn/dT is the temperature coefficient of refractive index, α is the thermal expansion coefficient, and $C_{r,\theta}$ is the function of elasto-optical coefficients P_{ij}.[6] ΔT is the temperature difference between the rod center and the surface and is related to the thermal focal length $f_{r,\theta}$, discussed in the previous section. For the Nd:YAG crystal with [111] orientation, the ΔT can be written as[6,8]

$$\Delta T = \frac{A}{4\pi L} \frac{1}{\left(\frac{1}{2} \frac{dn}{dT} + n_0{}^3 \alpha C_{r,\theta} \right)} \frac{1}{f_{r,\theta}} \quad (3a)$$

$$= \begin{pmatrix} 5.66 \times 10^4 (r) \\ 7.07 \times 10^4 (\theta) \end{pmatrix} \frac{R^2}{L} \frac{1}{f_{r,\theta}}. \quad (3b)$$

For the two-rod Nd:YAG laser, which includes a 90° quartz rotator between two crystal rods for the thermally induced birefringence compensation, the round-trip propagation matrix $\mathbf{M}_{p-p}$ for a plane–parallel resonator is given by

$$\mathbf{M}_{p-p} = \begin{bmatrix} A & B \\ C & D \end{bmatrix} \quad (4a)$$

$$= [d_1][M_r][l][d_R][l][M_\theta][d_1][d_1][M_\theta][l][d_R][l] \times [M_r][d_1], \quad (4b)$$

where $[d_1]$ is the propagation matrix for the distance d_1, $[l]$ is the propagation matrix for the distance between the crystal rod and the rotator, and $[d_R]$ is the propagation matrix for the rotator with the length d_R and refractive index n_R. Here, for the future use, we define the ray matrix $[d_2]$ for the distance between two crystal rods as

$$[d_2] = [l][d_R][l] = \begin{bmatrix} 1 & l \\ 0 & 1 \end{bmatrix} \begin{bmatrix} 1 & d_R/n_R \\ 0 & 1 \end{bmatrix} \begin{bmatrix} 1 & l \\ 0 & 1 \end{bmatrix} \quad (5a)$$

$$= \begin{bmatrix} 1 & 2l + d_R/n_R \\ 0 & 1 \end{bmatrix}. \quad (5b)$$

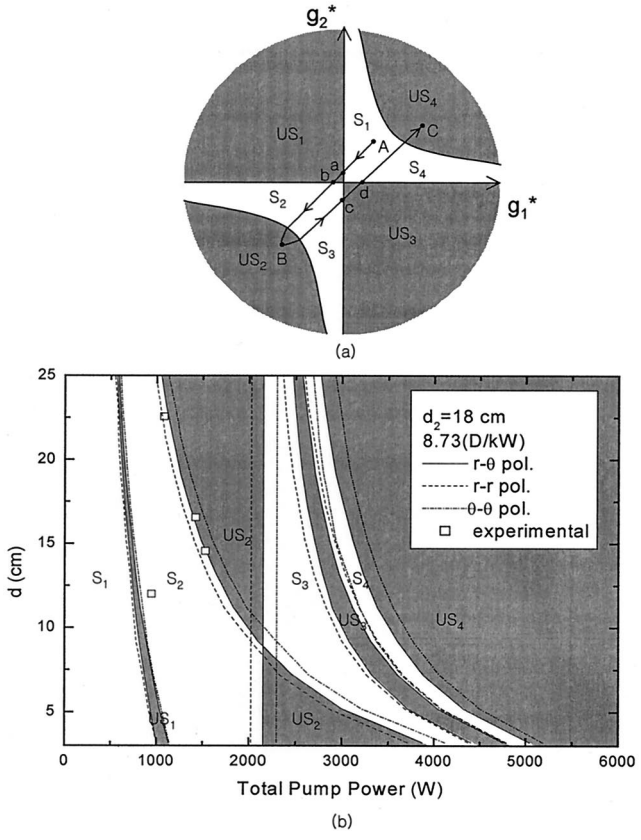

Fig. 2. Resonator stability condition (a) depicted schematically in the g_i^* plane, and (b) calculated with and without thermal birefringence compensation for a plane-parallel resonator with the short crystal rod separation of 18 cm and depicted in terms of a mirror distance (d_1) and total pump power.

For the plane–parallel resonator, single-pass matrix $\mathbf{M}_S$ is related to the length L^* and g_1^*, g_2^* parameters as follows:[3]

$$M_s = [d_1][M_r][l][d_R][l][M_\theta][d_1] \tag{6a}$$

$$= \begin{bmatrix} g_1^* & L^* \\ \dfrac{g_1^* g_2^* - 1}{L^*} & g_2^* \end{bmatrix}. \tag{6b}$$

From Eqs. (4a) and (4b), the stability condition of the resonator is given by

$$-1 < \frac{A + D}{2} < 1. \tag{7}$$

By using Eq. (7), we calculate the stability condition of the plane–parallel resonator in terms of the total input pump power of the two laser heads, the separation of the crystal rod, and the distance of the output coupler. The resulting stability condition calculated with the short crystal separation of d_2 = 18 cm is depicted in Fig. 2(b). For comparison, in Fig. 2(a) we added the stability condition depicted in the g_i^* plane. In our laser system with thermal birefringence compensation, an initial resonator stability condition in the g_i^* plane is located at the point (A) of the stable region S_1 for the total pump power corresponding to a laser threshold. Then, the resonator stability condition varies along a line connecting A–a–b–B–c–d–C for the increased pump power. The stable regions S_1, S_2, S_3, and S_4 of the g_i^*-plane correspond to the stable regions S_1, S_2, S_3, and S_4, respectively, depicted in Fig. 2(b). Similarly, the unstable regions US_1, US_2, US_3, and US_4 correspond to the darkened unstable regions US_1, US_2, US_3, and US_4, respectively, of Fig. 2(b).

The darkened unstable region US_1 shown in Fig. 2(b) was observed with thermal birefringence compensation and caused by the different focal length for the r and θ polarizations.[2] Thus the resonator condition with thermal birefringence compensation does not satisfy the condition of $g_1^* = g_2^* = 0$ by the different focal lengths $f_r \neq f_\theta$. However, without thermal birefringence compensation, the stability condition does satisfy the condition of $g_1^* = g_2^* = 0$, and the corresponding unstable condition of US_1 appears as a dashed curve between S_1 and US_1 for the r–r polarization, and also as a dashed-dotted curve between US_1 and S_2 for the θ–θ polarization. The unstable region US_2 is caused by the mirror distance d_1, which is not equal to the half-crystal separation $d_2/2$. Therefore the mirror distance d_1 needs to be equal to the half-crystal separation $d_2/2$ to minimize the width of the unstable region US_2. The unstable region US_2 corresponds to the unstable resonator condition near point B in Fig. 2(a).

For the more increased pump powers, the resonator condition returns along the line B–c–d–C and repeats stable and unstable conditions. Similar to the US_1, the darkened unstable region US_3 observed with thermal birefringence compensation is also caused by the different crystal focal lengths f_r and f_θ in the left side and the right side of the resonator. The unstable condition US_3 for the r–r polarization becomes a curve (not region) denoted as a dashed curve at the left side of the unstable region US_3, and that for the θ–θ polarization becomes also a curve denoted as a dashed-dotted curve at the right side of the US_3. The dashed curve existing between the US_3 and the above dashed-dotted curve at the right side of the US_3 corresponds to the unstable condition of US_4 for the r–r polarization. Note that the unstable region US_3 is broad in comparison with the US_1. From these resonator stability analyses with the short crystal separation of d_2 = 18 cm, one can see that stable laser operation is possible in the broad stable region S_2 up to the maximum total pump power of 2160 W for a mirror distance less than approximately 9 cm. Stable laser operation is limited by unstable region US_2 for mirror distances larger than 9 cm.

The resonator stability condition is modified for the increased crystal separation (d_2). Figure 3 shows the calculated stability condition of the resonator with the relatively long crystal separation of 39.2 cm. One major modification for the increased crystal separation is that the line a moves to the left-hand direction, and the resonator stability condition arrives

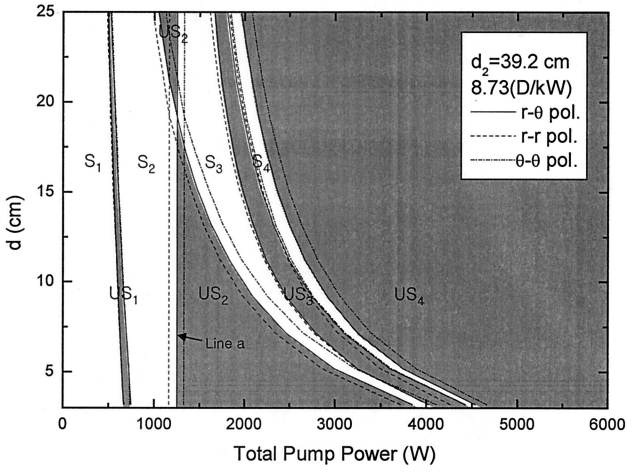

Fig. 3. Resonator stability condition of a plane-parallel resonator calculated with the ray-matrix method for the long crystal rod separation (d_2) of 39.2 cm.

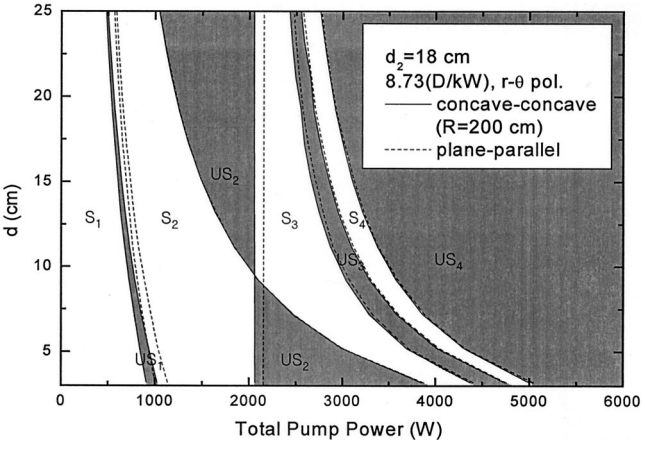

Fig. 4. Resonator stability condition of a concave-concave resonator calculated with the crystal rod separation of $d_2 = 18$ cm and both mirror radii of 200 cm.

at the unstable region US_2 for the low-input pump power. The broad stable operation range of the input pump power can be achieved only by positioning the mirror distance at $d_1 = d_2/2$. It is interesting to see that within our maximum pump power the unstable region US_2 can be utilized for stable laser operation. The long mirror distance can be utilized effectively in designing a resonator involving Q switched, nonlinear crystals, shutter, etc. For a plane–parallel symmetric resonator with two rods at no thermal birefringence compensation, the stable range of refractive power of one rod ($\equiv \Delta D_c$) has been known to be given by $8/L_R$ under the conditions of two crystal rods in the separation of $L_R/2$ and the crystal to mirror distance of $L_R/4$.[3] Here, L_R is the resonator length. In Ref. 3, the maximum point of the stable region corresponds to the resonator condition reaching the unstable region (US_4). However, for the resonator with thermal birefringence compensation, Fig. 3 shows that the stable range of refractive power can be limited by the unstable region (US_3), of which the width is broad and comparable with the stable region (S_4). In addition, the stable region (S_4) can be partially unstable by the unstable region (US_4) of the r–r polarization by incomplete thermal birefringence compensation. Therefore for the case of two rods placed in the separation of $L_R/2$ and the crystal-to-mirror distance of $L_R/4$, the maximum stable range is considered to be a little less than $(4 + 2\sqrt{2})/L_R$, which corresponds to the refractive power required to reach the center of unstable region (US_3).

For a concave–concave resonator with two rods at thermal birefringence compensation, the round trip propagation matrix M_{c-c} is given by

$$M_{c-c} = \lfloor R_f \rfloor [d_1][M_r][l][d_R][l][M_\theta][d_1][R_{oc}][d_1] \times [M_\theta][l][d_R][l][M_r][d_1], \quad (8)$$

where $\lfloor R_f \rfloor$ is the transfer matrix for the concave full mirror and $[R_{oc}]$ is that for the concave output coupler. Resonator stability condition can also be obtained by the relation given in Eq. (7), and the resulting stability condition is illustrated in Fig. 4. Here, both a full mirror and an output coupler are assumed to have the same radius of 200 cm, and $d_2 = 18$ cm. In comparison with the case of a plane–parallel resonator, the unstable region US_1 of the concave–concave resonator moves to the region of slightly lower input pump power. The unstable region (US_2) also moves to lower input pump power for the shorter mirror distance (d_1), less than ~9.5 cm. However, no change in lower limit of the unstable region US_2 is observed for the mirror distance longer than 9.5 cm. The minimum width of the US_2 exists at a slightly longer mirror distance of $d_1 = 9.5$ cm. Little changes are observed for the unstable regions US_3 and US_4.

3. Experimental Results

On the basis of the analysis of the stability condition described previously, we analyzed experimentally the characteristics of a plane–parallel resonator with two crystal rods with a 90° rotator in between. For the small gap distance with two crystal rods separated by $d_2 = 18$ cm, the laser output power is measured for the various mirror distances, as shown in Fig. 5. In the figure, total pump power represents the sum of input pump powers applied to two laser heads. The reflectance of an output coupler is fixed at 65% for this measurement. For the short mirror distance of $d_1 = 9$ cm, which corresponds to the $d_2/2$, the laser output power increases steadily in proportion to the total pump power, without any decrease in the output power. The maximum laser output power of 776 W corresponds to the optical efficiency of 45% and to the optical slope efficiency of 69%. However, as the distance d_1 of both laser mirrors is increased equally for the fixed crystal separation of 18 cm, the laser output power is saturated at high-input pump powers. The saturation points of total pump power exist at 1530 W for $d_1 = 14.6$ cm, 1422 W for $d_1 = 16.6$ cm, and 1080 W for $d_1 = 22.6$ cm. These input pump powers are depicted as empty squares in Fig. 2(b). We see that the

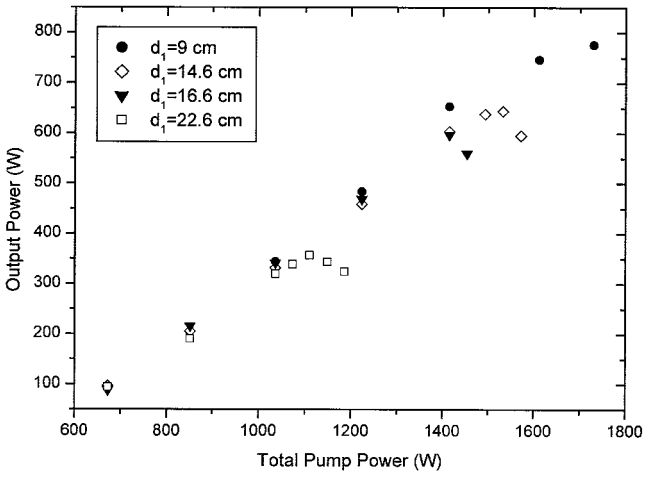

Fig. 5. Laser output power of a plane-parallel resonator measured for different mirror distances (d_1) with an output coupler reflectance of 65% and a crystal rod separation of d_2 = 18 cm.

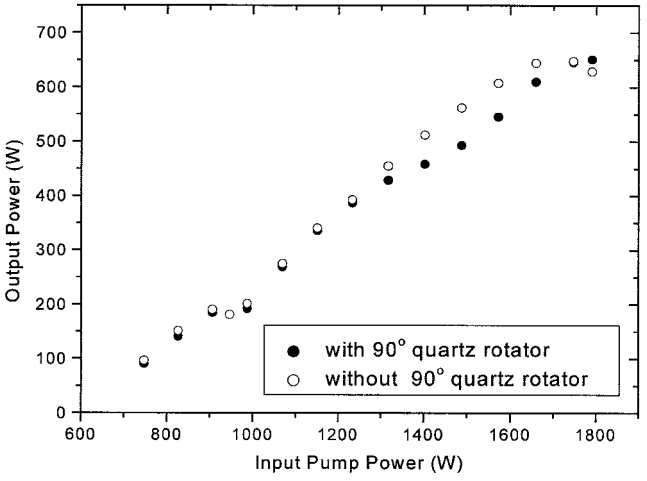

Fig. 7. Laser output power of a plane-parallel resonator measured with/without a 90° rotator at d_2 = 24.2 cm and d_1 = 12.1 cm.

saturation points measured experimentally coincide well with that of the calculated stability condition.

To see the laser output power characteristics of thermal birefringence compensated resonator at the stability condition of $g_1{}^*g_2{}^* = 0$, the laser output power of a plane–parallel and a concave–concave resonator are measured in detail, as shown in Fig. 6. For both resonators, the output coupler is placed at the short mirror distance of 9 cm, and the crystal rod separation is 18 cm. The radii of the concave–concave resonator are 200 cm. The laser threshold of a plane–parallel resonator existing at the total pump power of approximately 473 W indicates that initial stability condition belongs to the stable region S_1, shown in Fig. 2(a). However, around the stability condition of $g_1{}^*g_2{}^* = 0$, the laser output power of a plane–parallel resonator shows a narrow dip at the total pump power of approximately 1212 W. The narrow dip occurs inherently in the resonator with thermal birefringence compensation. Thus, as explained previously, the stability condition shown in Fig. 2(a) varies initially along a path A–a–b–B for the increased pump power. Even for the symmetric resonator with $d_1 = d_2/2$, the $g_1{}^*$ and $g_2{}^*$ parameters can not be zero simultaneously because the r- and θ-polarized beam experiences different crystal focal lengths in the left and right side of a resonator. This leads to the darkened unstable region US_1 of Fig. 2(b), and causes the narrow dip. Note that for the concave–concave resonator the narrow dip exists at a slightly lower input pump power of 1130 W.

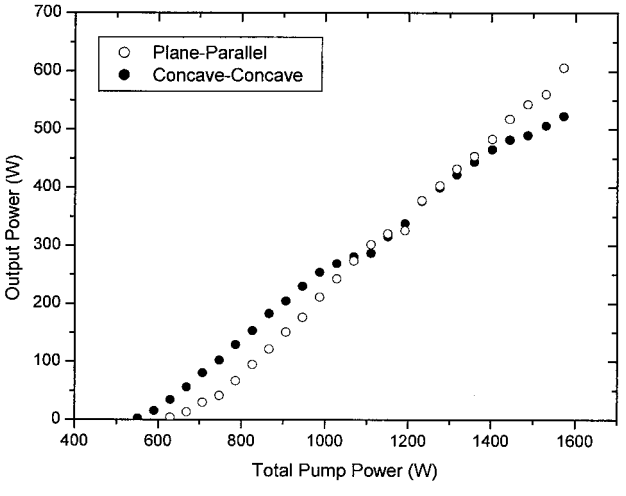

Fig. 6. Dependence of laser output power on total pump power measured with a short mirror distance of $d_1 = d_2/2$ = 9 cm for a plane-parallel and a concave-concave resonator. Reflectance of an output coupler is 65% for a plane-parallel and 70% for a concave-concave resonator.

As explained in Fig. 2(b), for the crystal rod separated at the short distance of d_2, a longer mirror distance is restricted by the unstable resonator condition US_2 in the range of high-input pump power. For a laser oscillator including a Q switch for pulsed operation and/or a second harmonic device for green beam generation, the long mirror distance is required while maintaining a high laser output power. One can achieve this by utilizing the third stable resonator condition S_3, shown in Fig. 3. To have a long mirror distance and to fully utilize the stable resonator condition without operating in the unstable region US_2, we construct a symmetric resonator with the long distances $d_1 = d_2/2$. Figure 7 shows the laser output power of a plane–parallel resonator measured with d_2 = 24.2 cm and d_1 = 12.1 cm. As expected, the laser power increases steadily up to the total pump power of 1620 W, and no power drop is observed at the resonator condition near US_2. This proves that a stable laser operation is possible in a symmetric resonator with d_2 = 24.2 cm and $d_1 = d_2/2$ = 12.1 cm. The narrow dip, which is observed at the relatively lower pump power of ~950 W in comparison with that for the short crystal separation of d_2 = 18 cm, can be explained by the unstable region US_1 moving to lower pump power range for the large crystal separation.

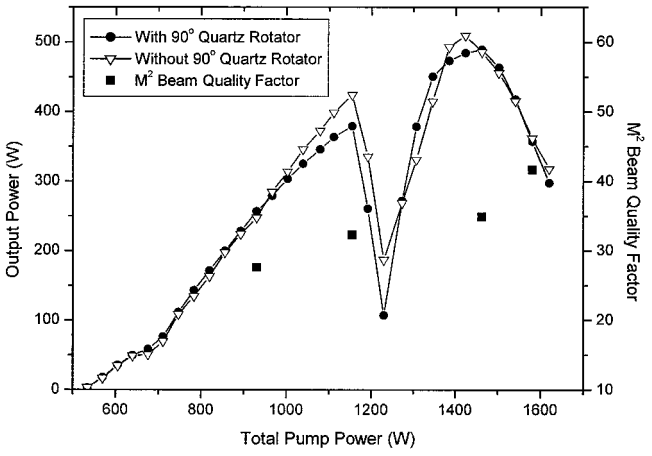

Fig. 8. Laser output power and M^2 beam quality factor of a plane-parallel resonator measured with a long crystal rod separation of $d_2 = 39.2$ cm and a mirror distance of $d_1 = 19.6$ cm.

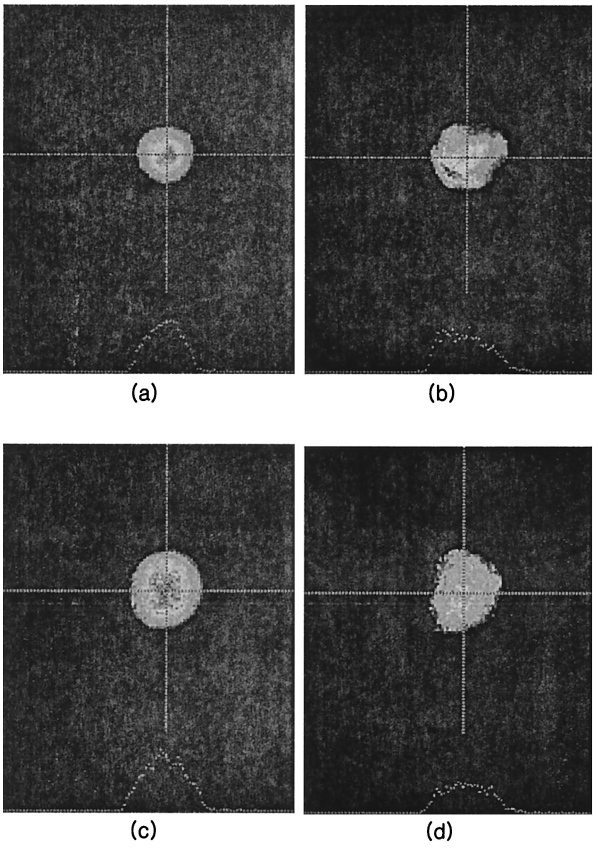

Fig. 9. Measured laser beam profiles depending on the stability conditions of the plane-parallel resonator. Beam profiles are measured at the total pump power of (a) 1151, (b) 1317, (c) 1572, and (d) 1746 W with $d_2 = 39.2$ and $d_1 = 19.6$ cm.

To investigate the laser behavior in the third unstable condition US_3, we construct a symmetric plane–parallel resonator with the long distances of $d_2 = 39.2$ cm and $d_1 = 19.6$ cm, which enable us to have US_3 within the range of the maximum total pump power. As shown in Fig. 8, the measured laser power decreases gradually for total pump powers above 1440 W by the third unstable condition US_3. Therefore for a symmetric resonator with thermal birefringence compensation, the stable range of a laser output power is limited by the unstable region US_3, and coincides with the theoretical stability analysis mentioned in Fig. 3. As expected, the narrow dip originated from an unstable condition US_1 moves further to the lower pump power range, and its effects to the laser output power are negligible. One interesting thing to note is that the laser output power drops at the total pump power of approximately 1224 W, which corresponds to the unstable region US_2. The power drop near the US_2 region may be caused by the increased sensitivity of laser power stability on the mechanical and/or thermal disturbances for the longer resonator length.

For the symmetric plane–parallel resonator constructed with the $d_2 = 39.2$ cm and $d_1 = 19.6$ cm, the laser beam profiles are measured to show the usefulness of the laser operation in the stable resonator condition S_3. For the beam-profile measurement a laser beam analyzer (Spiricon LBA-100A) equipped with a CCD detector (Pulnix TM-745E) was used, and the laser intensity was reduced with high reflective mirrors and neutral density filters. For the total pump power of 1572 W corresponding to the stable resonator condition S_3, the beam profile shows isotropic intensity distribution, as shown in Fig. 9(c). However, as shown in Fig. 9(d), the laser beam profile near the unstable resonator condition US_3 shows distorted intensity distribution for the increased pump power of 1746 W. Thus the stable operation range is limited by the US_3 owing to a decreased output power and a distorted intensity profile. Similarly, the beam profile has isotropic intensity distribution, as shown in Fig. 9(a) in the stable region S_2 with the corresponding pump power of 1151 W, and distorted intensity distribution, as shown in Fig. 9(b) near the unstable region US_2 with the corresponding pump power of 1317 W.

It is worth mentioning that the beam quality depends on a rotator. With a rotator between two crystal rods, better beam profiles are obtained with a slightly low M^2 beam quality factor. For the resonator with $d_1 = d_2/2 = 12.1$ cm, the M^2 beam quality factor of 61.9 is obtained with a rotator, while that of 63.8 is obtained without a rotator at the input pump power of 1790 W. As shown in Fig. 7, however, the laser output power is decreased slightly with the rotator owing to increased cavity loss, except the range of high pump powers, where the effect of thermal birefringence becomes severe and leads to saturation in laser output power.

We measured the M^2 beam quality factor of a plane–parallel and a concave–concave resonator for the varied mirror distance (d_1) and input pump power, and the results are shown in Fig. 10. The dependence of the M^2 beam quality factor on the mirror distance is measured with the $d_2 = 18$ cm and the input pump power of 1572 W. The mirror radii of the concave–concave resonator are 200 cm. Note

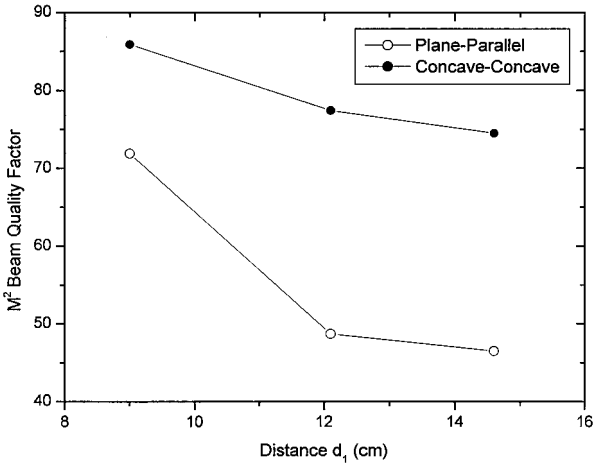

Fig. 10. Dependence of the M^2 beam quality factor on the mirror distance (d_1) measured for plane-parallel and concave-concave resonators with the input pump power of 1572 W and $d_2 = 18$ cm.

from Fig. 2(b) that the input pump power corresponds to the stable region S_2 for the d_1 less than approximately 15 cm. For the pump power of 1572 W in the region S_2, the M^2 beam quality factor is reduced as the mirror distance increases to the unstable region US_2. The measured M^2 value of a plane–parallel resonator was reduced from approximately 72 for $d_1 = 9$ cm to 45 for $d_1 = 14.6$ cm. Further reduction in the M^2 value is limited by unstable region US_2. For the concave–concave resonator, the measured M^2 value is approximately 86 for $d_1 = 9$ cm and is also reduced to 75 at $d_1 = 15$ cm.

For the fixed distances of $d_2 = 39.2$ cm and $d_1 = 19.6$ cm, we also measured the M^2 beam quality factor of a plane–parallel resonator as a parameter of the input pump power ranging from 747 to 1790 W. The measured M^2 values are denoted as darkened squares in Fig. 8. As depicted in Fig. 3, for $d_1 = d_2/2 = 19.6$ cm, the range of the input pump power corresponds to the stability condition ranging from the region S_2 to US_3. Near unstable regions US_2 and US_3, no noticeable reduction of the M^2 value is obtained owing to the unstable laser operation for the relatively long mirror distance. Therefore the laser operation near the unstable regions is not desirable for high-power lasers, owing to the large M^2 value and unstable laser operation. In the stable regions of S_2 and S_3, the M^2 value is increased slightly for the increased pump powers and is measured as approximately 35 in the S_3.

4. Conclusions

Using a matrix formula, we analyzed theoretically the stability condition of two laser heads with thermal birefringence compensation. The stability conditions of a plane–parallel and a concave–concave resonator were analyzed graphically in terms of a total pump power, a crystal rod separation, and a mirror distance. For the short crystal separation of $d_2 = 18$ cm, the resonator stability was analyzed as a stable condition up to our maximum input pump power of 2160 W for the mirror distances less than $d_1 = \sim 9$ cm. However, for the resonator with the $d_2/2 \neq d_1 > 9$ cm, the resonator stability condition was limited by the unstable region US_2 at high pump powers. In the experiment, the output power saturation due to the unstable region US_2 was observed, and its saturation point coincided with that predicted by the theoretical analysis.

For the resonator with a long crystal separation, the stable condition can be obtained with a symmetric resonator with $d_1 = d_2/2$. For the mirror distance of $d_1 = d_2/2$, the laser output power can be increased steadily up to the stable region S_3. However, we noted that the laser need hardly be operated stably above the stable region S_3, because the width of the unstable region US_3 is broad and compatible with that of the stable region S_4.

The unstable region US_1 of a concave–concave resonator was analyzed to occur at a lower input pump power in comparison with that of the plane–parallel resonator. Also, for the short mirror distance of $d_1 < 9.5$ cm, the lower boundary of US_2 of a concave–concave resonator exists at the slightly low input pump power compared with that of a plane–parallel resonator. However, little changes were observed in US_3 and US_4. We confirmed experimentally that the unstable region US_1 of a concave–concave resonator occurs at a lower input pump power in comparison with that of the plane–parallel resonator.

For a plane–parallel and a concave–concave resonator, we measured the M^2 beam quality factor for the varied mirror distance and the input pump power. The measured M^2 value of a plane–parallel was varied from ~ 72 for the $d_1 = 9$ cm to 45 for $d_1 = 14.6$ cm. However, for the concave–concave resonator, the measured M^2 value was measured to vary from 86 to 75 for the similar conditions.

References

1. Y. Akiyama, M. Sasaki, H. Yuasa, and N. Nishida, "Efficient high-power diode-pumped Nd:YAG rod laser," in *Conference on Lasers and Electro-Optics/Pacific Rim*, Vol. 1 of 2001 OSA Technical Digest Series (Optical Society of America, Washington, D.C., 2001), pp. 558–559.
2. K. Yasui, "Efficient and stable operation of a high-brightness cw 500-W Nd:YAG rod laser," Appl. Opt. **35,** 2566–2569 (1996).
3. K. P. Driedger, R. M. Iffländer, and H. Weber, "Multirod resonators for high-power solid-state lasers with improved beam quality," IEEE J. Quantum Electron. **24,** 665–674 (1988).
4. S. Lee, M. Yun, H. S. Kim, B. H. Cha, and S. Suk, "Output power and polarization characteristics for a diode side-pumped Nd: YAG laser with a diffusive optical pump cavity," Appl. Opt. **41,** 1082–1088 (2002).
5. S. Lee, S. K. Kim, M. Yun, H. S. Kim, B. H. Cha, H. J. Moon, "Design and fabrication of a diode side-pumped efficient Nd: YAG laser with a diffusive optical cavity for the laser output power of 500 W," Appl. Opt. **41,** 1089–1094 (2002).
6. W. Koechner, *Solid-State Laser Engineering*, 4th ed. (Springer, Berlin, 1996), Chap. 7, 398–402.
7. V. Mezenov, L. N. Soms, and A. I. Stepanov, *Thermooptics of Solid-State Lasers* (Mashinostroenie, Leningrad, 1986).
8. L. N. Somes, A. A. Tarasov, and V. V. Shashkin, "On the problem of depolarization of linearly polarized light by a YAG:Nd^{+3} laser rod under conditions of thermally induced birefringence," Sov. J. Quantum Electron. **10,** 350–351 (1980).